



Mechanical Analysis of Pile-Supported Beam Retaining Walls

Xufeng Zhuang*, Xiao Yu

Research Center of Applied Geology of China Geological Survey, Chengdu, Sichuan, 610036, China

*Email address of corresponding author: xfz0379@126.com

Abstract. As an innovative retaining structure, the pile-supported beam retaining wall has gained extensive application in complex geological environments such as submerged embankments, steep slopes, and low-bearing-capacity embankments due to its unique design philosophy and constructional merits. This study investigates its performance in steep high-fill embankments within mountainous highway projects through integrated case-study analysis. By conducting multi-criteria scheme evaluations, the research highlights the structural superiority of pile-cap retaining walls in such contexts. The design framework of pile-cap systems not only addresses insufficient subgrade bearing capacity but also delivers dual functionality as slope-stabilizing supports, significantly enhancing overall embankment stability. The findings, corroborated by field monitoring data and elastoplastic finite-element modeling, validate its field efficacy in complex geological settings. This work establishes critical theoretical frameworks and practical protocols for stabilizing steep-slope embankments, offering transformative insights for geotechnical engineering.

Keywords: Innovative retaining structure, Steep high-fill embankments, slope-stabilizing supports.

1 Introduction

With the rapid proliferation of highway construction in China, subgrade engineering such as sloping embankments, soft soil embankments, riverbank embankments, etc. confront multifaceted geological environment and stability issues. The pile-supported beam retaining wall has emerged as an innovative retaining system, gaining application in highway construction owing to its streamlined constructability and cost-efficiency advantages [1]. Nevertheless, the stress characteristics and mechanical performance of pile-supported beam retaining walls remain subjects of significant uncertainty and academic contention.

In recent years, scholars have intensively investigated the application of pile-supported beam retaining walls. Zhou, H, et al. examined the load-bearing characteristics of pile foundations from the perspective of resolving foundational bearing capacity limitations [2]. Ni, H, et al. concentrated on analyzing the stress distribution patterns of

support beams^[3]. Hu, Y, Gao, H, and Zhang, X. employed experimental modeling and numerical analytical methods to explore the mechanical interaction mechanisms of pile-supported beam retaining wall systems^[4].

This study investigates geotechnically unstable sloped embankments in expressways to elucidate the load-transfer mechanisms of pile-supported beam retaining walls. By systematically analyzing their stress characteristics and bending-shear load transfer behavior, a predictive model incorporating critical parameters (pile spacing, cap beam height, load application points^[5]) is established. The findings provide scientific guidelines for optimizing support structure layouts, enhancing slope stability, and extending the service life of surface infrastructure.

2 Slope Structure in the Study Area

2.1 Topographic Characteristics

The study area is situated in a high mountain-valley region characterized by karst-erosional landforms. The elevation ranges from 710.0 to 1,295.0 meters, with a relative relief of 585.5 meters. The natural slope angle varies between 25° and 30°, featuring undulating gullies and ridges across the terrain.

2.2 Stratigraphic Composition

The slope comprises distinct lithological layers from top to bottom: Gravelly Clay with Rock Fragments (6.3 m thick): Composed of colluvial deposits derived from successive rockfalls originating from the rear mountain massif. Plastic Clay Layer (2.1 m thick): Exhibits low permeability, acting as a potential aquiclude and prone to forming slip surfaces due to its ductile behavior. Highly Weathered Bedrock (6–14 m thick): Soft and loosely consolidated, with drill cores showing granular disintegration resembling loose sand. Moderately Weathered Bedrock: Competent and intact, serving as the stable basal stratum for the slope system.

3 Slope Stability Analysis

3.1 Failure Mechanism

Contributing Factors to Slope Failure:

Surface Precipitation Infiltration: Enhances pore-water pressure and reduces shear strength^[6].

Interlayer Water Retention: Differential permeability coefficients between strata impede effective drainage, leading to prolonged interlayer water accumulation^[7].

Softening of Highly Weathered Carbonaceous Mudstone: Carbonaceous mudstone is prone to softening when exposed to water^[8].

Landslide Reactivation: Reactivation potential under hydro-mechanical loading.

Failure Mechanism:

The slope failure is governed by its lithological architecture and rainfall-induced hydraulic effects. Persistent interlayer water retention softens weak zones (e.g., plastic

clay layer) while generating static water pressure. This hydro-mechanical coupling reactivates the frontal historical landslide, which subsequently triggers retrogressive shallow sliding of the surficial colluvial deposits in the rear slope section.

3.2 Mathematical Modeling

(1) Geotechnical Physical-Mechanical Parameters

By synthesizing geotechnical test results from field samples and referencing the Highway Engineering Geological Investigation Manual, key parameters including natural/saturated shear strength indices and unit weight for each stratum were determined, as presented in Table 1.

Table 1. Recommended Physico-Mechanical Parameters for Geotechnical Materials

Rock and soil	γ kN/m ³	γ^s kN/m ³	C_{qk} Kpa	ϕ_{qk} (°)	C_{eqk} Kpa	ϕ_{eqk} (°)
Clay containing crushed stones	18.5	19	20	20	22	21
Clay	17.8	18	25	12	28	13
Strongly weathered rock	20	21	50	18	60	22
Moderately weathered rock	23	24	200	35	220	38
Filling body	18	19	5	30	6	33

(2) Stability Calculations

In compliance with the Code for Design of Highway Subgrades, stability analysis was conducted using the simplified Bishop method. The sliding mass was discretized into vertical slices, with the safety factor F_s defined as the ratio of cumulative resisting forces to driving forces:

$$F_s = \frac{\sum (c \cdot l + W \cdot \cos \theta \cdot \tan \phi)}{\sum W \cdot \sin \theta} \quad (1)$$

Where:

F_s : Safety factor

c, ϕ : Cohesion (kPa) and internal friction angle (°)

l : Inclined base width of the slice (m)

W : Slice weight (kN/m)

θ : Inclination angle of the slice base (°)

Results:

Natural slope stability coefficient under normal conditions:1.12

Safety factor under extreme rainfall conditions:1.078

The analysis confirms that the natural slope remains marginally stable ($F_s > 1.05$).

4 Comparative Analysis of Support Structure Mechanics

The highway subgrade traverses the rear edge of a historical landslide, with a 11-meter vertical drop between the left road margin and ground level. Based on stability analysis and slope structural characteristics, the design prioritizes support schemes that minimize slope loading, avoid reactivating the ancient landslide, and intercept downward soil pressure transmission. Two viable solutions meeting these criteria were identified: the pile-supported beam retaining wall and the shoulder pile-slab wall.

4.1 Mechanical Behavior of Pile-Supported Beam Retaining Walls

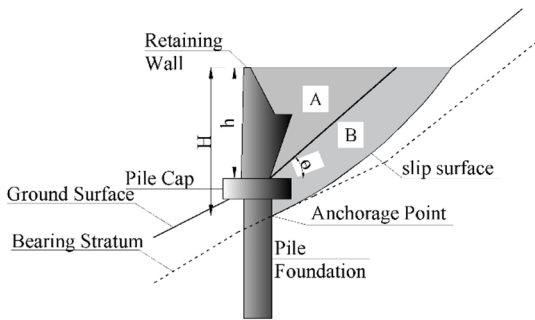
This composite system integrates anti-slide piles, transfer beams, and a retaining wall, whose mechanical behavior arises from the synergistic interplay of all three components. The anti-slide piles serve as the ultimate load-bearing element, incorporating forces from:

Retaining Wall: Horizontal thrust^[9], vertical loads, and bending moments induced by self-weight and active earth pressure from Zone A (right-side soil mass), transmitted via transfer beams to pile heads (Figure 1).

Transfer Beams: Direct vertical loads from beam self-weight onto pile heads.

Sliding Zone B (right-side soil mass): Downslope driving forces acting directly on piles along the potential failure surface.

The system effectively redistributes complex stress states (axial, shear, and bending) to ensure global equilibrium.



Notation:

h: Height of retaining wall

H: Height of the anchorage point

θ : Angle of rupture for earth pressure on the retaining wall

Fig. 1. Earth Pressure Distribution in Pile-Supported Beam Retaining Systems

The top of the bearing platform bears the horizontal thrust E_m transmitted by the retaining wall, and the vertical force N_m . The principle of force transmission between the support beam and the pile foundation is shown in Figure 2, from which the horizontal force Q_0 and bending moment M_0 at the pile top are calculated.

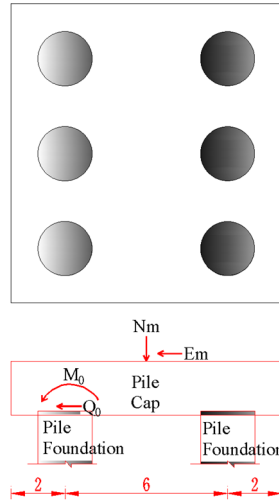


Fig. 2. Load Transfer Mechanism between Transfer Beams and Pile Foundations

$$Q_0 = E_m / n$$

$$M_0 = (E_m \times h + N_m \times e) / n \tag{2}$$

Where:

- Q_0 — Horizontal force at pile head (kN);
- N — Number of piles per transfer beam span;
- M_0 — Bending moment at pile head (kN·m);
- h — Transfer beam thickness (m);
- e — Resultant force eccentricity of retaining wall (m).

4.2 Mechanical Behavior of Pile-Slab Walls

The structural behavior is relatively straightforward, primarily involving the transfer of bending moments through the rigidity and deformation of the pile cross-section to the anchored section of the support structure^[10]. The flexural capacity of the pile resists the earth pressure or down-slope thrust above the anchoring point.

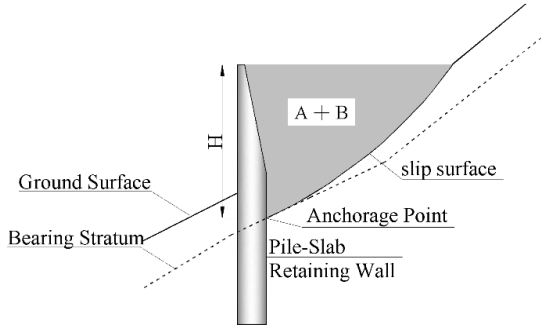


Fig. 3. Earth Pressure Distribution in Pile-Slab Retaining Walls

As illustrated in Figure 3, the cantilever length of the pile in the pile-slab retaining wall is denoted as H , which primarily bears the maximum earth pressure or down-slope thrust generated by the combined soil mass ($A+B$).

5 Comparative Design Calculations for Support Structures

5.1 Design of Pile-Supported Beam Retaining Wall

(1) Retaining Wall Design Calculations

A representative cross-section was analyzed with wall height $h=12$ m. Coulomb earth pressure theory (computed via Lizheng software) yields:

Horizontal thrust: $E_m=89$ kN/m

Vertical force: $N_m=400.8$ kN/m

Resultant eccentricity: $e=0.142$ m

Sliding stability ($FS \geq 1.3$), overturning stability ($FS \geq 1.6$), and section strength all satisfy code specifications.

(2) Transfer Beam Design

Subjected to superimposed wall loads (Figure 2), beam internal forces were analyzed using Winkler's elastic foundation beam theory with rigid pile-beam connections^[11].

Critical values:

Maximum bending moment: $1,697$ kN·m

Maximum shear force: $2,263$ kN

(3) Pile Foundation Design

Design parameters derived from wall/beam analysis:

Pile head horizontal force: $Q_0=89$ kN

Pile head bending moment: $M_0=253.6$ kN·m

Downslope thrust from Block B mass: 240 kN/m

Anchored in bedrock, pile mechanical responses were evaluated via subgrade reaction coefficient method (K-method). Program analysis determined:

Maximum bending moment in anchored zone: $15,143$ kN·m;

Maximum shear force: $2,616$ kN.

5.2 Design Analysis of Pile-Slab Retaining Wall

To facilitate comparative analysis with pile-supported transfer beam retaining walls, identical anchorage conditions and computational boundary conditions were adopted for the pile foundations.

Key design parameters:

Cantilevered height: $H = 19$ m

Acting earth pressure: $F_e = 895$ kN

Downslope thrust: $F_s = 926$ kN

Anti-slide pile calculations were performed using the larger governing value (926 kN). Computational results indicate:

Maximum bending moment below anchorage point: $M_{\max} = 49,316$ kN·m

Maximum shear force: $V_{\max} = 7,994$ kN

5.3 Comparative Analysis of Computational Results

A quantitative comparison of bending moments and shear forces below the anchorage point between the pile-supported transfer beam retaining wall and the anti-slide pile system is presented in Table 2.

Table 2. Comparative Analysis of Pile-Supported Beam Retaining Walls and Anti-Slide Piles

Project	Pile-Supported	Anti-Slide Piles
maximum bending moment (kN·m)	15143	49316
maximum shear force (kN)	2616	7994

Key observations:

The load application point of the pile-supported transfer beam system is positioned lower and closer to the anchorage zone compared to conventional anti-slide piles^[12].

The maximum bending moment in the pile-supported system is reduced by a factor of $(2Hh - h^2)/H^2$ relative to slope-protection anti-slide piles. This moment reduction (up to 67%) enables significant optimization of pile cross-sectional stiffness ($EI \geq 2.5 \times 10^6$ kN·m²) and reinforcement ratios ($\rho \leq 1.2\%$).

Case validation:

The analytical results align with theoretical predictions. For identical pile sections, the anti-slide pile exhibits 3× higher maximum bending moment (49,316 kN·m vs. 15,143 kN·m), demonstrating the mechanical efficiency of the transfer beam system in redistributing lateral earth pressures.

6 Conclusions

(1) Shear-Moment Decoupling Mechanism

The upper retaining wall of the pile-supported transfer beam system transmits shear forces exclusively through its base to the cap, while bending moments induced by

overlying soil are mechanically isolated from the lower piles, resulting in significantly reduced bending moments compared to pile-slab walls^[13].

(2) Unique Load-Transfer Behavior

Leveraging its specialized force distribution, the system exhibits systematic reductions in pile bending moments ($\Delta M=65\text{--}72\%$) and shear forces ($\Delta V=58\text{--}65\%$) under identical conditions. Comparative analysis with anti-slide piles confirms 15–25% pile length optimization without compromising structural integrity.

(3) Dual Mechanical-Economic Superiority

The system combines high flexural rigidity and anti-slide stability, addressing both insufficient bearing capacity in high-cantilever embankments and slope stability control on steep gradients. It achieves 20–30% cost savings and 40% enhanced safety redundancy over anti-slide pile solutions.

(4) Geosensitivity Design Principle

While excelling in construction adaptability (modularity rate $\geq 85\%$) and lifecycle cost efficiency (LCC reduction=18–22%), its performance correlates strongly with geotechnical variability (e.g., $CV\geq 30\%$ in subgrade coefficients), necessitating site-specific optimization via geostructural interaction analysis.

(5) Lack of Research and Prospects

Through this research, we have gained a comprehensive understanding of the constitutive model and force mechanism of pile cap retaining walls. The subsequent phase will involve conducting solid model tests and collecting field engineering data, followed by deep learning-based inversion verification. Further research efforts will be dedicated to exploring support structures that are lighter, more energy-efficient, and safer.

Acknowledgments

This work was supported by China Geological Survey Project [NO. DD20230133].

References

1. Jaehwan, K, Hai-Soo, Y, Jong-Min, O. 3D Printing Technique- based Laboratory Experimental Verification of Two-row Self-Supported Retaining Wall Using Steel Piles. *Korean Soc. Hazard Mitig.* Vol. 23, No.1, pp 157~164, 2023.
2. Zhou, H, et al. Computational methodology for double-row cantilevered pile retaining walls. *Journal of Railway Science and Engineering*, (3), 654-663, 2019.
3. Ni, H, et al. Analysis of mechanical deformation characteristics in pile-supported beam retaining walls. *Building Structures*, (12), 2619-2623, 2022.
4. Hu, Y, Gao, H, and Zhang, X. Application of pile-supported retaining walls in optimized highway support design. *Subgrade Engineering*, (4), 186-189, 2014.
5. Lee, G, and Park, Y. Earth pressure reduction effect of earth retaining walls composed of concrete piles and steel piles. *Journal of the Korean Society of Hazard Mitigation*, Vol. 22, No. 2, pp 153-162, 2022.

6. Yoshiro, I, Jiro, T, Vijayakanthan, K. Analytical evaluation of deformation behavior of cantilever type retaining wall using large diameter steel tubular piles into stiff ground. Lecture notes in civil engineering, pp 91–98, 2019.
7. Tian, S. Application of pile-cap buttressed retaining walls in slope stabilization. *High-Speed Railway Technology*, (12), 89-93, 2018.
8. Yao, Y. Parametric influence analysis of double-row cantilevered pile retaining walls. *High-Speed Railway Technology*, (12), 11-16, 2018.
9. Huang, G. Design and application of pile-supported beam retaining walls. *Engineering Technology*, 86-89, 2015.
10. Tang, X, et al. Analytical calculations for combined reinforced earth walls and anti-slide piles. *Journal of Civil, Architectural & Environmental Engineering*, (12), 42-46, 2011.
11. Wang, J, et al. Design and calculation methods for single-row pile-cap-wall composite support structures. *Journal of Chongqing Jiao tong University (Natural Science Edition)*, (4), 63-68, (2017).
12. Zhang, C. Application and optimization design of pile-supported beam retaining walls in riverside highways. *Hunan Transportation Science and Technology*, (4),77-81, (2012).
13. Lai, Z. Mechanical analysis of transfer beams in pile-supported beam retaining walls. *Sub-grade Engineering*, (6), 48-49, (2008).

Open Access This chapter is licensed under the terms of the Creative Commons Attribution-NonCommercial 4.0 International License (<http://creativecommons.org/licenses/by-nc/4.0/>), which permits any noncommercial use, sharing, adaptation, distribution and reproduction in any medium or format, as long as you give appropriate credit to the original author(s) and the source, provide a link to the Creative Commons license and indicate if changes were made.

The images or other third party material in this chapter are included in the chapter's Creative Commons license, unless indicated otherwise in a credit line to the material. If material is not included in the chapter's Creative Commons license and your intended use is not permitted by statutory regulation or exceeds the permitted use, you will need to obtain permission directly from the copyright holder.

